

# Accounts of Materials & Surface Research

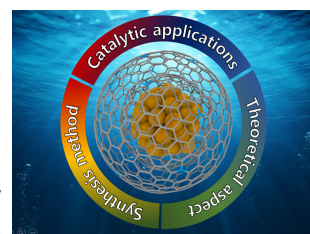
## Understanding of metals encapsulated in carbon layers and their electrocatalytic applications

Seung Hyo Noh<sup>a</sup>, Jeemin Hwang<sup>a</sup>, Byungchan Han<sup>a\*</sup> and Takeo Ohsaka<sup>b\*\*</sup>

<sup>a</sup>Department of Chemical and Biomolecular Engineering, Yonsei University, Seoul, 03722, Republic of Korea \*bchan@yonsei.ac.kr

<sup>b</sup>Research Institute for Engineering, Kanagawa University, 3-27-1, Rokkakubashi, Kanagawa-ku, Yokohama, Japan \*\* ohsaka1950@gmail.com

Nanoscale metallic particles encapsulated in N-doped carbon layers (M@N-C) are reviewed on the aspect of electrocatalytic application. It is pointed out experimentally and theoretically that their catalytic activity is engaged with several key descriptors such as encapsulating carbon layer thickness, heteroatom doping level and alloying species in the core of the particle. Furthermore, novel design principles for tuning the electrocatalytic performance far beyond conventional Pt are proposed.



**Keyword:** Electrochemical catalyst, encapsulation, activity, durability, non-precious catalyst

**Dr. Seung Hyo Noh** received his Bachelor's and Master's degrees from Hanbat National University and DGIST, Republic of Korea, respectively. He earned his PhD in the Department of Electronic chemistry at the Tokyo Institute of Technology, Japan in 2016.



**Jeemin Hwang** is a graduate student at the Department of Biomolecular and Chemical Engineering, Yonsei University. She obtained her bachelor's degree in the Department of Chemistry at the University of Minnesota. Her research is focused on the catalyst for metal-air battery and fuel cell. Her research interest is to design bi-functional catalysts for the hydrogen evolution reaction or oxygen evolution and reduction reaction using density functional theory simulations.



**Dr. Byungchan Han** is an Associate Professor at the Department of Chemical and Biomolecular Engineering of Yonsei University in Seoul, Korea. He earned his PhD degree in MIT at the Dept. of Materials Science and Engineering in 2007. He obtained Bachelor and Mater degrees from the Dept. of Nuclear Engineering of Seoul National University. He spent two years in MIT and another two years in Stanford University as a Postdoctoral Research Associate.



**Takeo Ohsaka** received his PhD degree from Tokyo Institute of Technology (TIT) in 1981 and worked as a postdoc at Caltech (1981-1982), an assistant professor at Tokyo Univ. of Agri. & Tech. (1982-1990) and then an associate/ full professor at TIT (1990-2016, professor emeritus). He is now a visiting professor of Research Institute for Engineering at Kanagawa University. His major research is focused on electrocatalysts for ORR, OER, HER, HOR, etc., in fuel(biofuel) cells, water electrolysis, Li-O<sub>2</sub> battery and on bio/electroanalytical sensors, reactive oxygen species (ROSs) and water treatments by AOP.



# Understanding of metals encapsulated in carbon layers and their electrocatalytic applications

Seung Hyo Noh<sup>a</sup>, Jeemin Hwang<sup>a</sup>, Byungchan Han<sup>a\*</sup> and Takeo Ohsaka<sup>b\*\*</sup>

<sup>a</sup>Department of Chemical and Biomolecular Engineering, Yonsei University, Seoul, 03722, Republic of Korea

<sup>b</sup>Research Institute for Engineering, Kanagawa University, 3-27-1, Rokkakubashi, Kanagawa-ku, Yokohama, Japan

## 1. Introduction

Chemical reactions are vital for sustaining human beings in modern society via harvesting energy and producing various chemical goods [1-3]. In general, the process of any chemical reaction is controlled by interplay of thermodynamics for net outcomes and kinetics for the rate. It is hard to imagine, in practice, that any chemical reaction proceeds without employing catalysts due to substantial activation barriers to reach the transition state from reactant state, in spite of thermodynamic spontaneity toward product state. Thus, the reason to search for highly active catalysts, which effectively low the activation energy and enhance the desired yield, is essentially engaged with saving substantial amounts of energy and monetary costs in chemical reactions.

In the electrochemical reactions involving with the electron transfer at electrodes (anode and cathode), the utilization of electrochemical catalysts (electrocatalysts) is inevitable for practical applications. Among a variety of electrocatalysts, Pt-based catalysts have been widely and significantly studied in that these catalysts are not only relatively stable, but also active in severe (e.g., acidic or alkaline) media. As one of examples, bulk Pt metal is stable as high as 1.188 V vs. SHE [4], while the other metals such as Fe (-0.44 V), Co (-0.28V) and Ag (0.799 V) are easily dissolved below the potential. Although a gold metal is known as durable until 1.52 V bulk Au-based materials are chemically inert, and thus inappropriate for electrocatalysts. Hence, costly Pt-based catalysts have been still unique candidates in both activity and durability aspects for

various electrochemical applications such as oxygen reduction reaction (ORR), oxygen evolution reaction (OER), hydrogen evolution reaction (HER) and so on. However, it is of difficulty to widely commercialize them due to expensive material costs and sustainable supply of Pt.

To overcome these issues, a variety of synthetic methods were attempted. For instance, Pt-alloy catalysts such as Pt-Co, Pt-Ni and Pt-Fe have shown superior activities to pure Pt counterpart, saving the material cost by substituting Pt with other inexpensive 3d-metals [5-9]. Chen et al. [10, 11] suggested the preparation of the Pt-Ni alloy with a high performance and kinetic current density through careful structure control of the material to maximize the catalytic surface area and to properly alloy the elements. The control of particle size has been also claimed for an effective utilization of the surface area, and it is known experimentally that the appropriate particle size is 3~4 nm [12, 13]. However, amount of Pt content in catalysts is still problematic in commercialization of Pt-based catalysts.

In the recent advances of research, non-precious (or Pt-free) catalysts have been extensively studied as the alternatives of Pt. There are three representative types of non-precious catalysts: 1) a non-precious metallic catalyst showing an outstanding activity in acidic solution. Zelenay and associates [14-16] have demonstrated that a nitrogen-doped polyaniline driven iron catalyst (PANI-Fe-C) with a macrocyclic structure can be active and durable toward ORR. 2) metal oxide catalysts which are of great promise in the metal-air battery or alkaline fuel cell system. Dai et al. revealed that a cobalt oxide supported on nitrogen-doped reduced

graphene oxide ( $\text{Co}_3\text{O}_4/\text{N}_{\text{rm}}\text{-Gr}$ ) is useful for a bi-functional catalysis toward ORR and OER in metal-air battery [17]. 3) a metal-free catalyst which is also another family of non-precious counterpart. It has been of interest to develop it into non-precious catalysts because these kinds of materials are free from the issue of metal dissolution. In general, nitrogen-doped carbon materials such as nitrogen-doped graphene (N-Gr) [18-21], nitrogen-doped carbon nanotube (N-CNT) [22-26], nitrogen-doped fullerene (N-fullerene) [27, 28] have been broadly highlighted besides heteroatom-doped metal-free catalysts such as (N, P) [29] or (N, S) [30, 31] in alkaline media. On the other hand, the issues from durability and activity in acidic media constrain their uses in a variety of catalytic applications.

As the one of state-of-the-art catalytic materials, a metal encapsulated in N-doped carbon ( $\text{M@N-C}$ ) attracts focused attention since the metal is protected by carbon shells, and the catalyst consists of relatively cheap and sustainable components such as nitrogen, carbon and metals (Fe, Ni, Co, and so on). Furthermore, the metal in carbon shells can be substituted by a variety of materials. For instance, metal oxide, metal carbon and metal alloy can be encapsulated to tune the catalysis, implying that  $\text{M@N-C}$  structures can be optimized for a wide range of electrochemical catalysis.

In this review, we comprehensively introduced recent experimental progresses on the electrocatalytic activity of  $\text{M@N-C}$  type catalysts and theoretical understandings of their electrocatalysis and their design principles.

## 2. Catalytic applications of $\text{M@N-C}$ materials

### 2.1 Hydrogen evolution reaction

The electrochemical evolution of hydrogen has been attracting strong attention due to its energy carrier feature. In particular, the sustainable supply of hydrogen in a proton exchange membrane fuel cells (PEMFCs) is essential to obtain electrical energy, keeping environmentally clean products and high efficiency. As stated in the Introduction, expensive Pt-based catalysts are still one of the best electrocatalysts for HER so far. Identification of alternative to Pt with cheaper

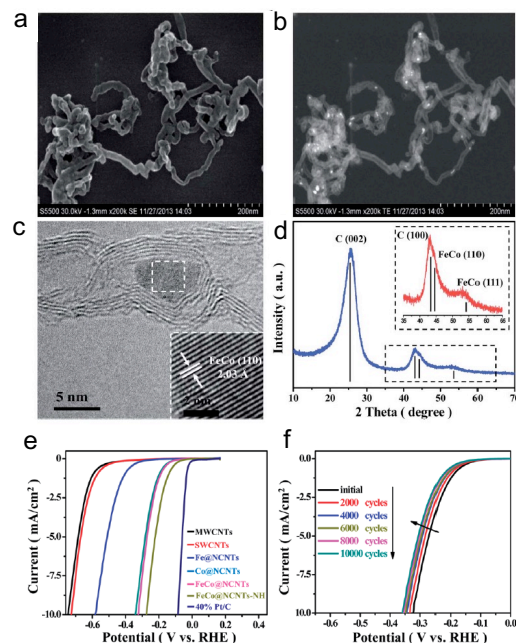
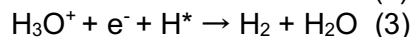
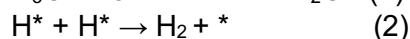


Fig. 1. a. SEM image, b. STEM image and c. HRTEM image of FeCo@NCNTs with the inset showing the (110) crystal plane of the FeCo nanoparticle. d. XRD pattern of FeCo@NCNTs with the inset showing the partially enlarged detail between 35 degrees and 65 degrees. e. Polarization curves of Fe@NCNTs, Co@NCNTs, FeCo@NCNTs, FeCo@NCNTs-NH along with MWCNTs, SWCNTs and 40% Pt/C. f. Durability measurement of FeCo@NCNTs. Adapted with permission from ref. 37, RSC.

materials such as transition metal dichalcogenide [32], metal pyrites [33, 34] and metal phosphides [35, 36] has been extensively and intensively attempted. It was known that the catalysts in acidic media facilitate production of hydrogen gas from hydronium ions via mechanisms consisting of Volmer, Tafel and Heyrovsky steps as shown by eqs. (1) ~ (3), respectively [37].



where \* represents the adsorption site and  $\text{H}^*$  the adsorbed H. Each of the reaction steps shows different Tafel slope and it was theoretically evaluated as 29 (Volmer step), 38 (Tafel step), 116 mV/dec (Heyrovsky step)

[38]. Considering that the Tafel slope of Pt/C catalyst is approximately 37 mV/dec, the Tafel step (equation 2) should be the rate-determining one. The intermediate of adsorbed hydrogen atom ( $H^*$ ) plays a key role in the mechanism and kinetics of the HER.

In addition to a high activity, an electrocatalyst should possess a long-term stability. On this aspect, M@N-C materials can be one of the promising HER catalysts. Deng et al. suggested the concept of carbon encapsulation of metals using nitrogen-doped bamboo-like carbon nanotubes (FeCo@NCNTs) as shown in Fig. 1a-c [37]. They synthesized approximately 5 nm sized FeCo nanoparticles encapsulated in carbon nanotube and the XRD peaks correspond to FeCo nanoparticle as shown in Fig. 1d. FeCo@NCNTs catalyst showed a superior catalytic performance (onset potential ( $E_{\text{onset}}$ ):  $\sim 70$  mV vs. RHE) while multi-walled carbon nanotubes (MWCNTs) and single-walled carbon nanotubes (SWCNTs) without core metals presented high overpotentials approximately  $-0.75$  V vs. RHE at  $10 \text{ mAcm}^{-2}$ , and it is largely negative compared to the  $E_{\text{onset}}$  ( $\sim 0.1$  V) of 40 wt% Pt/C as indicated in Fig. 1e. It was reported that FeCo@NCNTs treated with  $NH_3$  at  $1000^\circ\text{C}$  (FeCo@NCNTs-NH) showed better HER activity ( $\sim 70$  mV vs. RHE) than single metal encapsulated catalysts such as Fe@NCNTs and Co@NCNTs. It implies that the combination of alloying metals is able to activate the outermost carbon surface. The Tafel slope obtained for FeCo@NCNTs-NH is about 72 mV/dec. These values suggest that HER obeys the Heyrovsky mechanism as written by eq. (3). FeCo@NCNTs catalyst indicates a high durability as well as a good activity. In the durability test, FeCo@NCNTs showed the potential drop of only 50 mV at  $10 \text{ mAcm}^{-2}$  during 10,000 cycles (Fig. 1f).

Figure 2a-d shows typical encapsulation structures suggested by Tavakkoli et al. [39]. They synthesized single-shell carbon-encapsulated iron nanoparticles (SCEINs). The SCEINs had relatively homogeneous particle size of 5 nm and were dispersed on a single wall carbon nanotube (SWCNT). SCEIN catalyst is of a rational design in that iron particle is encapsulated in a single carbon layer, and its catalysis occurs on the

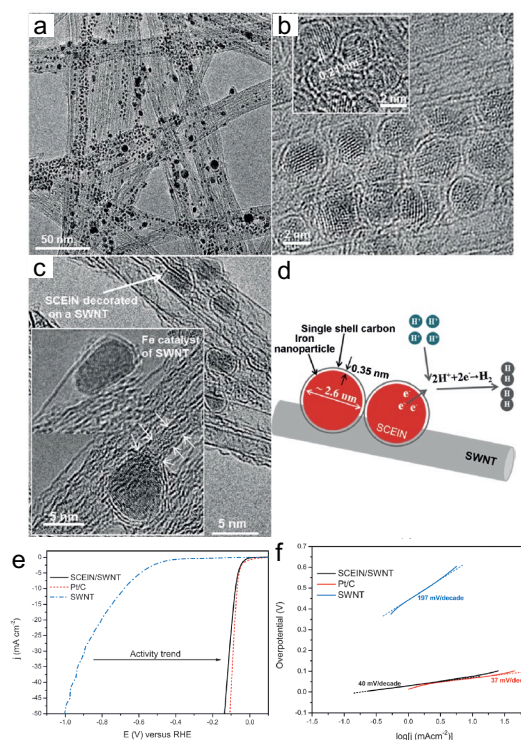


Fig. 2. a. TEM image and b. HRTEM image of SCEINs supported on SWNTs showing distribution of the particles on the SWNTs with the inset indicating the (110) lattice plane of the Fe particles in SCEINs. c. HRTEM image of SCEINs decorated on the sidewalls of the SWNTs, the inset shows Fe catalyst particles for the growth of the SWNTs. d. Schematic representation of SCEIN/SWNT sample simplifying the HRTEM images and HER on SCEINs. e. The polarization curves and f. the corresponding Tafel plots of SWNT (blue), SCEIN/SWNT (black), and Pt/C (red). Adapted with permission from ref. 39, Wiley.

surface of catalyst. The carbon shell is pointed out as an active site assuming that metal is totally encapsulated in carbon shell and not exposed to the electrolyte solution.

The thinner the carbon shells are, the stronger hydrogen adsorption intensity is. Accordingly, the single-layer encapsulation may lead to better catalytic performance than multi-shell M@N-C catalyst, if there is issue of weak hydrogen adsorption at thick carbon shells. In the theoretical part of this study, the carbon thickness effect on the catalysis is discussed in detail. In the experimental observations, the HER was enhanced via the SCEIN/SWNT combination as shown in Fig. 2e, and this catalyst is comparable to the performance of Pt/C catalyst. The SCEIN/SWNT catalyst includes SWNT support, but the SWNT shows a poor

catalytic activity, i.e.,  $E_{\text{onset}} = \sim 0.4$  V vs. RHE. Hence, it is suggested that the HER catalysis of the SCEIN/SWNT mainly occurs on the SCEIN catalyst.

The Tafel slope obtained for the SCEIN/SWNT (40 mV/dec) is similar to that of Pt (37 mV/dec) rather than SWNT (197 mV/dec) (see Fig. 2f). The low Tafel slope of 40 mV/dec shows that the initial hydrogen adsorption is fast, and the rate-determining step is the Heyrovsky step as eq. (2) (the electrochemical desorption of hydrogen molecules) and the overall reaction obeys the Volmer-Heyrovsky mechanism.

## 2.2 Oxygen reduction and evolution reactions

The encapsulated structures as HER catalysts have been especially focused among their electrochemical applications [40-42]. The applications of M@N-C catalysts are,

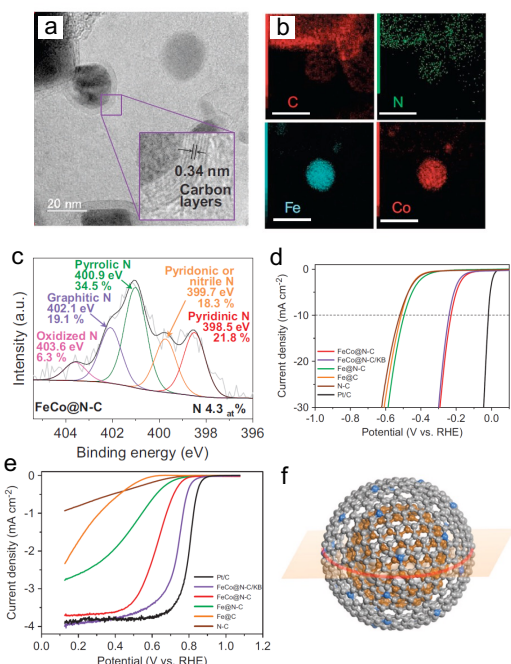


Fig. 3. Structural analysis of FeCo@N-C and theoretical model of M@N-C catalysts. a. TEM images of FeCo@N-C/KB catalysts. b. Elemental mapping of C, N, Fe and Co by energy-dispersive X-ray spectroscopy. c. Core level N 1s XPS of FeCo@N-C catalyst. d-e. HER and ORR polarization curves for FeCo@N-C, FeCo@N-C/KB, Fe@N-C, Fe@C, N-C and Pt/C. f. Illustration of metal@N-C nanoparticle. Adapted with permission from ref. 44, Nature.

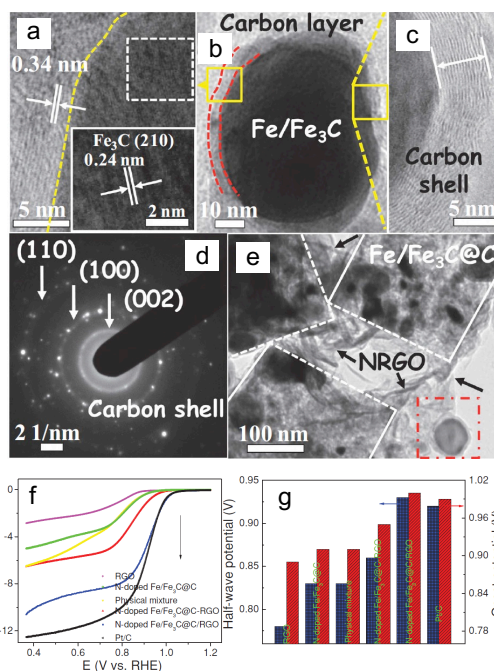


Fig. 4. TEM images, SAED patterns, and HRTEM images of a-d. N-doped Fe/Fe<sub>3</sub>C@C, and e. N-doped Fe/Fe<sub>3</sub>C@C/RGO. f. LSV curves of RGO, N-doped Fe/Fe<sub>3</sub>C@C, physical mixture, N-doped Fe/Fe<sub>3</sub>C@C-RGO, N-doped Fe/Fe<sub>3</sub>C@C/RGO and Pt/C. g. The corresponding half-wave potentials and onset potentials of RGO, N-doped Fe/Fe<sub>3</sub>C@C, physical mixture, N-doped Fe/Fe<sub>3</sub>C@C-RGO, N-doped Fe/Fe<sub>3</sub>C@C/RGO and Pt/C. Adapted with permission from ref. 46, Wiley.

however, not limited to HER [43]. Oxygen reduction reaction (ORR) is also one of the substantially studied reactions using them. In particular, it is not easy to develop a non-precious catalyst toward ORR in acidic environments since it has to satisfy both the activity and durability at the same time. A M@N-C catalyst, however, is expected to be free from the durability issue once metal particles are encapsulated in carbon shells, because the metal dissolution may be prevented.

Noh et al. [44] synthesized FeCo@N-C catalyst for both HER and ORR in a variety of candidate materials such as Co@N-C and Fe@N-C based on the DFT calculations on their catalytic activity as indicated in Fig. 3d,e. FeCo nanoparticles were encapsulated in carbon shells, and the inner metals were analyzed using energy dispersive spectroscopy (EDS) and X-ray photoelectron

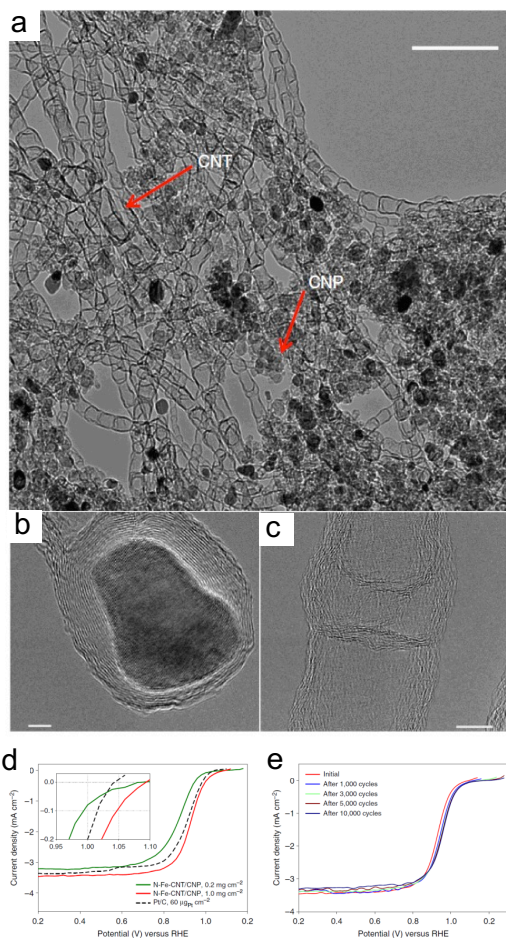


Fig. 5. Micrographs of carbon nanotube/nanoparticle composite. a. HTEM of the N-Fe-CN/CNP composite catalyst. b. Iron encapsulated in graphene nanoshells. c. Typical bamboo-like defect in graphene. d. ORR polarization curves before cycling durability test. e. ORR polarization curves measured during cycling durability. Scale bar, 10 nm. Adapted with permission from ref. 47, Nature.

spectroscopy (XPS) as indicated in Fig. 3a-c. In the outer carbon shells of M@N-C nanoparticle, graphitic, pyrrolic and pyridinic N are observed. It was known that in planar nitrogen doped graphene the pyridinic N is preferred to graphitic or pyrrolic N, since the N atoms are dominantly located in the edges of the graphene sheet. On the other hand, the metal encapsulation structures do not include such edges owing to their spherical shape (typically shown in Fig. 3f) except for the defects of their carbon shell. This structural feature has an advantage to prevent the electrochemical corrosion resulting from altering the electronic structure of surface carbon.

In general, Fe-based materials have been utilized as carbon-capsulated materials. Hu et al. [45] reported that iron carbide ( $\text{Fe}_3\text{C}$ ) encapsulated by carbon, possessed a superior activity and electrochemical stability over the cycling tests. The carbon-coated

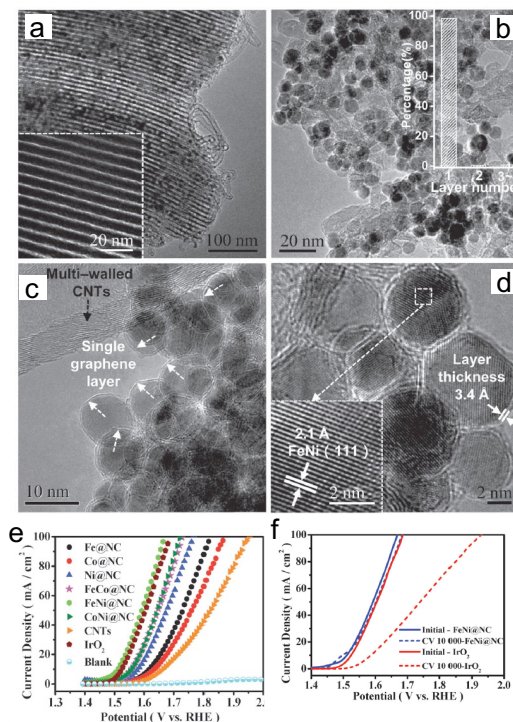


Fig. 6. Morphology and structural characterizations of M@NCs. a. TEM images of FeNi@NC/SBA-15 with the inset indicating the image of pure SBA-15. b–d. HRTEM images of FeNi@NC. The inset in b. is a statistical analysis of the layer number of the graphene shell on metal nanoparticles. The white arrows in the inset of c. show the single layer graphene and the black arrow in the inset of c. shows the multi-walled carbon nanotubes. The inset in d. shows the (111) crystal plane of the FeNi alloy and the graphene layer with a layer thickness of 3.4 Å. e. OER polarization curves for M@NCs in comparison with CNTs and  $\text{IrO}_2$  with the same mass loading. f. Durability test of FeNi@NC in an alkaline electrolyte in contrast to  $\text{IrO}_2$ . Adapted with permission from ref. 49, RSC.

metals are utilized in not only acidic but also alkaline media. Hou et al. reported the ORR catalysis of N-doped carbon coated iron carbide (N-doped  $\text{Fe}/\text{Fe}_3\text{C}@C$ ) [46]. Their TEM images and RDE results demonstrated that this type of catalysts can be applied to alkaline fuel cells and metal-air batteries as presented in Fig. 4a-g.

Chung et al. synthesized N-Fe-CNT/CNP catalyst via a simple heat-treatment as indicated in Fig. 5a-c [47], in which carbon nanotube (CNT) and carbon nanoparticle (CNP) were formed at the same time. This strategy seems attractive because the N-Fe-CNT support can enhance the electric conductivity as well as the catalysis itself of the spherical catalyst (N-Fe-CNP). The N-Fe-CNT/CNP shows a high  $E_{\text{onset}} = 1.16$  V vs. RHE as shown in Fig. 5d. Its activity is even higher than that of PtNi catalyst ( $E_{\text{onset}} = 1.05$  V vs. RHE) [48].

On the other hand, Bao et al. reported the FeNi encapsulated in N-doped carbon (FeNi@N-C) for oxygen evolution reaction (OER) (Fig. 6a-d.) [49]. They tried to include a variety of metal elements as inner cores such as FeCo, FeNi, CoNi as well as single metals of Fe, Co and Ni. FeNi@NC catalyst shows even better catalytic activity for OER than  $\text{IrO}_2$  [50], which is known as one of the best OER catalysts. In particular, it indicates a high durability in alkaline solution (at 1 M NaOH solution) at high potential of 1.51 V vs. RHE at  $10 \text{ mAcm}^{-2}$ .  $\text{IrO}_2$  catalyst shows the large potential drop of 70 mV at  $10 \text{ mAcm}^{-2}$  during 10,000 cycles (-0.46 and 0.54 V (vs. Hg/HgO) at  $100 \text{ mVs}^{-1}$  at the initial and 10,000<sup>th</sup> cycles, respectively) as shown in Fig. 6 e,f, while FeNi@NC catalyst shows a negligible potential loss. This study demonstrates that a proper selection of alloying elements can be easily designed for various desired catalysis, and the carbon capsulation may bring about their long-term stability [51].

### 3. Aspect of theoretical analysis

Typically, metal and nitrogen coordinated carbon materials, so-called metal complexes or macrocyclic structures [14, 52], are broadly studied as electrocatalysts experimentally and theoretically because they show a superior performance in electrocatalysis to the conventional non-precious catalysts. For example, Zelenay and his associates proved that polyaniline driven Fe complex (PANI-Fe-C) possesses an extraordinary electrocatalytic activity for ORR, i.e., this material showed the onset-potential of 0.93 V (vs. SHE) and also the half-wave potential of 0.81 V compared to 0.85 V of Pt/C.

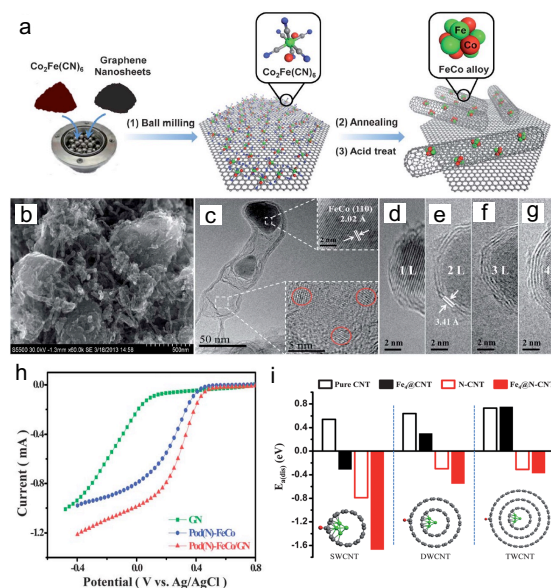


Fig. 7. a. Schematic illustration of the synthesis process of Pod(N)-FeCo/GNs from the precursor  $\text{Co}_2\text{Fe}(\text{CN})_6$  and graphene nanosheets, where gray balls represent C atoms, blue for N, green for Fe, and red for Co. b–g. Morphology analysis of Pod(N)-FeCo/GNs ( $m(\text{GN})/m(\text{Co}_2\text{Fe}(\text{CN})_6) = 0.5 : 1$ ): b. SEM image; c. TEM image, the top inset shows the (110) crystal plane of the FeCo alloy and the bottom inset shows the smaller FeCo nanoparticles encapsulated within the compartments of the pod-like CNTs; d–g. HRTEM images showing the cross-sections of FeCo nanoparticles covered by one to four layers of graphitic carbon walls (1L–4L). h. RDE polarization curves of Pod(N)-FeCo/GNs ( $m(\text{GN})/m(\text{Co}_2\text{Fe}(\text{CN})_6) = 0.5:1$ ). i. The DFT calculated dissociative adsorption energy of  $\text{O}_2$  ( $E_{\text{a}}(\text{dis})$ ) on the carbon surface of pure or N-doped (two nitrogen atoms doped) SWCNTs, DWCNTs, and TWCNTs with or without an enclosed  $\text{FeN}_4$  cluster. Adapted with permission from ref. 62, RSC.

The electrocatalysis of these types of catalysts has been studied based on a variety of theoretical calculations. For instance, Kattel et al. [53] studied the ORR electrocatalysis of nitrogen-coordinated Fe-macrocyclic catalyst ( $\text{FeN}_4$ ) using first principles density functional theory (DFT) [54–57]. The active site of  $\text{FeN}_4$  catalyst is pointed out as Fe atom site, not nitrogen or carbon [58]. The rate-determining step of ORR is the dissociation step of OOH. The dissociated O and OH are located at Fe atom and carbon site, respectively and the activation barrier of the dissociation is  $\sim 0.6$  eV.

Furthermore, N-doped graphene materials also were proposed intensively as alternatives to Pt catalyst due to their abundant material resources. The active site of N-doped graphene is different from that of the  $\text{FeN}_4$  catalyst. Pyridinic N has been suspected as an active site, not pyrrolic and graphitic N. Guo et al. provided an experimental evidence for this. They synthesized highly oriented pyrolytic graphite (HOPG) carbon, in which the edges are functionalized with pyridinic-N (pyri-HOPG) or graphitic-N (grap-HOPG). The active catalytic site was considered as pyri-HOPG rather than grap-HOPG. The wider edge area of pyridinic N exposed, the higher catalytic activity is. Many theoretical calculations supported the observations [20, 59-61]. It is interesting that the active sites are changed by the material

structure in spite of similar carbon-based materials. Therefore, it is imperative to understand the fundamental underlying reaction mechanism and characteristic of structures for enhancing a catalytic activity and durability.

On the other hand, there are only a few researches of N-doped carbon coated metals (M@N-C) in both experiments and theoretical calculations despite their potential catalytic applications. Deng et al. [62] insisted that the number of carbon shell affects the catalytic activity of nitrogen-doped carbon coated metals using bamboo-like CNT structures (Fig. 7). The ORR activity may decrease with increasing the carbon shell number as shown in the theoretical study (Fig. 7i). It is very interesting since it means that their catalysis can be controlled by the thickness of the carbon shells. This study was concentrated on ORR, but the concept may be also transferable for other reactions. Such a carbon shell thickness effect on electrocatalysis is one of special properties distinguished from 2D materials such as N-graphene or  $\text{FeN}_4$  macrocyclic structure. Furthermore, the encapsulation structures have fruitful perspectives to tune catalytic activities by alloying of core metals, nitrogen doping of carbon shell and changing the carbon layer thickness.

Noh et al. [63] elucidated the underlying mechanism of the emergence of active catalysis in an encapsulated configuration. They modeled the nitrogen-doped carbon using metal supports (N-Gr/M), and in this case the slab model was found to be beneficial to identify effect of metal species decoupling the surface curvature and edge factors. Supporting metals affect the electronic structure of N-doped graphene, being observed by the charge distribution and Bader charge techniques. The inner metal atoms donate electrons to the outer carbons nearby the doped N, and the electrons are shared with the reaction intermediate, oxygen atom. This strengthens the oxygen binding relatively compared to the pristine graphene or N-doped graphene.

Interestingly, the type of core metals was found to be important in determining the binding energy, distance between metal and N-Gr and electronic structures, namely N-Gr/Cu catalyst is a promising catalyst among a variety of 3d transition metals such as Ni,

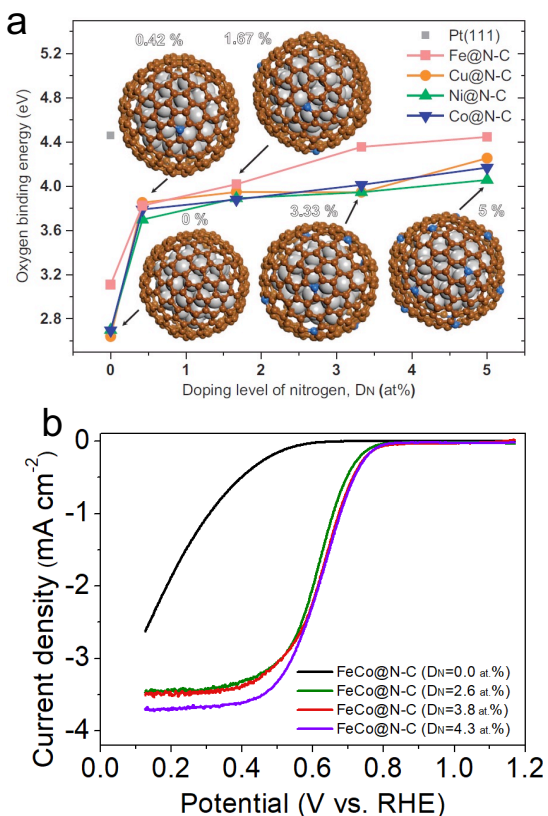


Fig. 8. Nitrogen-doping model and oxygen binding energy on M@N-C. a. Oxygen binding energies on M@N-C (M=Fe, Cu, Ni and Co) as a function of DN, typically 0, 0.42, 1.67, 3.33 and 5 at.% and Pt(111) for comparison. b. ORR performance of FeCo@N-C catalysts as a function of N-doping level (DN). The samples with DN = 0.0, 2.6, 3.8 and 4.3 at.% were synthesized using ammonium sulfate of 0, 200, 400 and 600 mg, respectively. Adapted with permission from ref. 44, Nature.

Co and Fe. However, this planar N-Gr/Cu material is not practical for catalytic application in that it needs to be synthesized as a nanoparticle to utilize a high surface area.

To demonstrate the ORR activity of N-Gr/Cu catalyst, subsequently, we fabricated Cu@N-C, with the Cu particles encapsulated in nitrogen-doped carbon shells using simple hydrothermal and heat treatments [64]. After the heat treatment, its ORR catalytic activity was measured as poor even in alkaline electrolyte (0.1 M KOH solution). However, this catalyst could be activated by CO<sub>2</sub> treatment. The TEM images and EDS elemental mapping showed that the synthesized materials are covered with thick carbon layers and thus have a low ORR activity. On the other hand, CO<sub>2</sub> treatment led to an enhanced activity as a result of the oxidation of carbon shells (i.e., due to the decrease in the shell thickness) by CO<sub>2</sub> as a mild oxidant at high temperature.

Theoretical calculations suggested that Cu@N-C possesses a proper oxygen binding energy (3.82 eV) compared to pure Cu nanoparticle structure (5.30 eV) and N-doped graphene (3.43 eV). Thus, it turned out that carbon encapsulation opens a way to control the interaction between inner metal and oxygen atoms adsorbed on the carbon shell. In the pristine metal (herein Cu), oxygen strongly interacts with Cu probably forming metal oxide, while in N-doped carbon shell oxygen shows a weak binding energy. According to the well-known Sabatier principle, too weak and too strong oxygen bindings lead to rate-determining steps at the initial and late ORR catalysis, respectively.

The researchers carried out experiments to validate the DFT calculations and identified three factors to tune oxygen binding, a key factor of ORR activity: 1) carbon thickness, 2) alloying and 3) nitrogen doping effects [44].

They also investigated oxygen binding energy of Fe@N-C as a function of nitrogen doping level and found that N-doping level is important to intensify oxygen binding energy. Fe@N-C catalyst weakly adsorbs oxygen (~3.1 eV) without N doping but with a marginal doping concentration, the binding was strengthened dramatically. Figure 8a shows the oxygen binding energy of 3.8 eV at 0.42 at%

N doping level ( $D_N$ ) and the oxygen binding energies at M@N-C ( $M = \text{Fe, Co, Ni, Cu}$ ) seem to be saturated at 4.4 eV at  $D_N = 5$  at%, which is close to the experimental

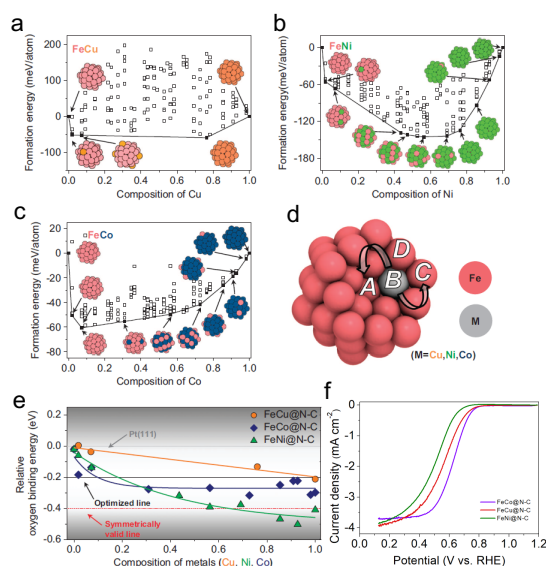


Fig. 9. Alloying effect of M@N-C catalysts via DFT calculations and experimental observations. Energy convex hulls of a. FeCu, b. FeNi and c. FeCo nanoparticles. d. Segregation model in FeM nanoparticle. The segregated positions are the core of nanoparticle (A), vertex (C), edge (D) or sublayer (B, not segregated). e. Relative oxygen binding energies on FeM@N-C nanoparticles as a function of the composition of second metal (M). f. ORR performance in accordance with alloy species such as FeCo, FeNi and FeCu@N-C catalysts ( $D_N \approx 4\%$ ). Oxygen binding energies are represented as  $E(\text{FeM@N-C}) - E(\text{Pt}(111))$ , where  $E(\text{FeM@N-C})$  and  $E(\text{Pt}(111))$  are oxygen binding energies on FeM@N-C and Pt (111), respectively. Adapted with permission from ref. 44, Nature.

observation (~ 5 at%). Higher N-doping levels may enhance oxygen binding, but then, it is more difficult to synthesize. Doped N is also found to activate the nearest-neighboring carbon atoms. These outcomes well agree with experimental results. The carbon-coated iron without N doping shows the lowest ORR activity as shown in Fig. 8b. The higher N-doping level is, the higher (close to optimal value) performance is.

As mentioned above, the carbon thickness is one of important factors to control the surface properties of catalyst. The binding interaction between metal and oxygen is reduced by increasing the number of carbon layers. It is noteworthy that it is important to

possess thin 4~5 layers of carbon shells in order to manifest a good catalytic feature of the interaction with the outer carbon shells. The effect of the carbon layers well appears using a single layer carbon coating [37, 39, 49, 62].

Another way to manipulate the binding energy of oxygen adsorbate is to change the metal species and the alloying compositions. It was known that the oxygen binding energy is correlated with the kinds of metals. For instance, N-Gr/Fe shows a strong binding compared to N-Gr/(Co, Ni and Cu) for the same number of carbon layers [63]. Fig.9 shows the alloying effect of M@N-C catalysts as a function of metal composition via energy convex hull calculations for FeCo@N-C, FeNi@N-C and FeCu@N-C catalysts [44]. Alloys of 3d transition metals such as Ni, Co, and Cu show weak binding energies with oxygen atom. In accordance with the trend, a proper composition can create better oxygen affinity compared to Pt (111) surface. Interestingly, FeCo@N-C catalyst indicates a good performance in the all composition range, while FeNi@N-C shows a lower catalytic activity at the high Ni composition over 0.65 due to its too weak oxygen binding as shown in Fig. 9e,f.

Carbon-coated catalysts have been studied significantly in HER, ORR and ORR. They could be further applied to a variety of catalysis with high activity and durability, by careful design of metal alloys, metal oxides and metal carbides as inner materials encapsulated by carbon shells.

#### 4. Synthesis of single-layer carbon coated metals

Metal encapsulation catalysts are fabricated using sustainable and abundant materials such as carbon, nitrogen and non-precious metals (such as Cu, Ni, Fe and Co). Ohsaka and his associates synthesized the carbon-coated metal catalysts using sugar (or glucose), ammonium sulfate, and metal salts, which were the precursors of carbon, nitrogen, and metals, respectively [44, 64].

As stated above, the catalytic activity of metal encapsulation materials can be tuned by carbon thickness, nitrogen doping level, and alloying species and compositions.

In general, nitrogen doping and metal compositions are controlled relatively readily

using appropriate amounts of nitrogen and metal precursors. On the other hand, it is difficult to control carbon thickness. The precise control of carbon thickness may enhance electrocatalytic performance. Chen

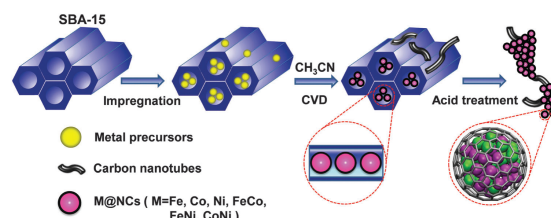


Fig. 10. Schematic illustration of the synthesis process of M@NCs from metal-containing precursors and SBA-15. Adapted with permission from ref. 49, RSC.

et al. tried to synthesize pure carbon nanotubes without an impurity [29]. In their synthesis, Fe nanoparticles were utilized as a catalyst to grow carbon nanotube from CH<sub>4</sub> gas. They found that several metal catalysts were coated on the carbon sources and then, the carbon-coated metals were formed. The carbon coating on particles was not removed in spite of acid treatment. This fact suggests that carbon-coated metallic catalysts are of a rational design in acidic electrochemical conditions due to being free from instability issue for a long-term operation compared to other 3d-metals or metal oxides. The carbon coating can be eliminated by CO<sub>2</sub> treatment at high temperature [29, 64], which informs us of an idea to reduce the number of carbon layers (from the top layer) coating inner metals or metal oxides (which may be considered as a “top-down catalyst synthesis”)

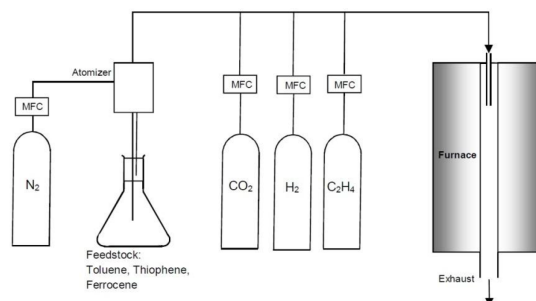


Fig. 11. A scheme of the synthesis reactor used for the growth of SCEIN/SWNT. Adapted with permission from ref. 39, Wiley.

On the other hand, Cui et al. suggested a “bottom-up synthesis method” of

electrocatalysts [49]. They utilized the ordered mesoporous silica template (SBA-15) to limit the thickness of carbon shell and regulate particle size as shown in Fig. 10. This method is useful in preparing single-layer graphene encapsulating metals. This layer-controlled catalyst shows a superior catalytic activity in the water oxidation in alkaline solutions.

Tavakkoli et al. proposed fast and low-cost aerosol chemical vapor deposition method for a one-step synthesis of single-shell carbon-encapsulated iron nanoparticle (SCEINs) catalyst toward HER, which were decorated on single-walled carbon nanotubes (SWNTs). A vertical furnace system (Fig. 11) was used in their method, in which ferrocene, toluene and thiophene were purged as precursors with N<sub>2</sub> gas to react in the furnace within a short time. The carbon-coated metals sank to the bottom of furnace by their gravity. In general, an electric furnace is set up in parallel with a static alumina crucible and in this case the precursors are located in the inner side of the furnace during a long time for heating and cooling processes. On the contrary, the method employed by Tavakkoli et al. is very attractive for mass production because carbon-coated metals can be fabricated in continuous process as long as supply of precursors. The synthesized SCEIN/SWNT catalyst shows a comparable HER performance to Pt/C catalyst.

The above-mentioned procedures allow us to control the carbon thickness of carbon-coated metal catalysts and finally obtain a single-layer carbon coating which is an important factor to achieve optimal catalytic activity.

## 5. Conclusions

In this study, we discussed the catalytic applications of carbon-coated nanometals, the theoretical understanding of their catalytic activity and their synthesis. The carbon-coated metal materials have a resistance to acidic solution and also a variety of factors to tune their electrocatalytic activities. Hence, a variety of carbon layer-encapsulated catalysts can be utilized in various (electro)chemical catalysis. Furthermore, the thickness, alloying composition and nitrogen doping level are

important factors to tune their catalytic activity and to achieve a better catalytic activity. In particular, the synthesis and analysis of single-layer carbon-coated catalysts are very interesting from a viewpoint of achieving optimal catalytic activity.

Theoretical calculations help to elucidate the catalytic activity, active site, mechanism (electron transfer between carbon and metal). On the other hand, to completely understand and enhance them, the experimental demonstration should be carried out.

## 6. Acknowledgement

This study was supported by the Ministry of Education, Culture, Sports, Science and Technology (MEXT), Japan and the National Research Foundation of Korea (NRF). This research was mainly supported by the Global Frontier Program through the Global Frontier Hybrid Interface Materials (GFHIM) of the National Research Foundation of Korea (NRF) funded by the Ministry of Science and ICT (2013M3A6B1078882). Also this research was funded by the New & Renewable Energy Core Technology Program of the Korea Institute of Energy Technology Evaluation and Planning (KETEP, Grant No. 20173010032080).

## References

- 1) A. Harb, *Renewable Energy*, (2011), 36, 2641-2654.
- 2) J. Kang, B. Han, *ACS Appl. Mater. Interfaces*, (2015), 7, 11599-11603.
- 3) J. Kang, J.-S. Yu, B. Han, *J. Phys. Chem. Lett.*, (2016), 7, 2803-2808.
- 4) M. Pourbaix, Atlas of electrochemical equilibria in aqueous solutions, Pergamon 1966.
- 5) E. Antolini, J.R. Salgado, E.R. Gonzalez, *J. Power Sources*, (2006), 160, 957-968.
- 6) H.A. Gasteiger, S.S. Kocha, B. Sompalli, F.T. Wagner, *Applied Catalysis B: Environmental*, (2005), 56, 9-35.
- 7) V.R. Stamenkovic, B. Fowler, B.S. Mun, G. Wang, P.N. Ross, C.A. Lucas, N.M. Marković, *Science*, (2007), 315, 493-497.
- 8) P. Strasser, S. Koh, T. Anniyev, J. Greeley, K. More, C. Yu, Z. Liu, S. Kaya, D. Nordlund, H. Ogasawara, *Nat. Chem.*, (2010), 2, 454.
- 9) L. Xiong, A. Kannan, A. Manthiram, *Electrochemistry Communications*, (2002), 4, 898-903.
- 10) C. Chen, Y. Kang, Z. Huo, Z. Zhu, W. Huang, H.L. Xin, J.D. Snyder, D. Li, J.A. Herron, M. Mavrikakis, *Science*, (2014), 343, 1339-1343.
- 11) Y. Wang, Y. Chen, C. Nan, L. Li, D. Wang, Q. Peng, Y. Li, *Nano Res.*, (2015), 8, 140-155.

- 12) N. Muthuswamy, J.L.G. de la Fuente, P. Ochal, R. Giri, S. Raaen, S. Sunde, M. Rønning, D. Chen, *Phys. Chem. Chem. Phys.*, (2013), 15, 3803-3813.
- 13) F. Şen, G. Gökağaç, *J. Phys. Chem. C*, (2007), 111, 5715-5720.
- 14) G. Wu, K.L. More, C.M. Johnston, P. Zelenay, *Science*, (2011), 332, 443-447.
- 15) F. Jaouen, E. Proietti, M. Lefèvre, R. Chenitz, J.-P. Dodelet, G. Wu, H.T. Chung, C.M. Johnston, P. Zelenay, *Energy Environ. Sci.*, (2011), 4, 114-130.
- 16) C.W. Bezerra, L. Zhang, K. Lee, H. Liu, A.L. Marques, E.P. Marques, H. Wang, J. Zhang, *Electrochim. Acta*, (2008), 53, 4937-4951.
- 17) Y. Liang, Y. Li, H. Wang, J. Zhou, J. Wang, T. Regier, H. Dai, *Nat. Mater.*, (2011), 10, 780.
- 18) L. Qu, Y. Liu, J.-B. Baek, L. Dai, *ACS Nano*, (2010), 4, 1321-1326.
- 19) L. Lai, J.R. Potts, D. Zhan, L. Wang, C.K. Poh, C. Tang, H. Gong, Z. Shen, J. Lin, R.S. Ruoff, *Energy Environ. Sci.*, (2012), 5, 7936-7942.
- 20) L. Zhang, Z. Xia, *J. Phys. Chem. C*, (2011), 115, 11170-11176.
- 21) R.I. Jafri, N. Rajalakshmi, S. Ramaprabhu, *J. Mater. Chem.*, (2010), 20, 7114-7117.
- 22) K. Gong, F. Du, Z. Xia, M. Durstock, L. Dai, *Science*, (2009), 323, 760-764.
- 23) C.V. Rao, C.R. Cabrera, Y. Ishikawa, *J. Phys. Chem. Lett.*, (2010), 1, 2622-2627.
- 24) D. Guo, R. Shibuya, C. Akiba, S. Saji, T. Kondo, J. Nakamura, *Science*, (2016), 351, 361-365.
- 25) Z. Chen, D. Higgins, Z. Chen, *Carbon*, (2010), 48, 3057-3065.
- 26) Z. Chen, D. Higgins, H. Tao, R.S. Hsu, Z. Chen, *J. Phys. Chem. C*, (2009), 113, 21008-21013.
- 27) F. Gao, G.-L. Zhao, S. Yang, J.J. Spivey, *J. Am. Chem. Soc.*, (2013), 135, 3315-3318.
- 28) S.H. Noh, C. Kwon, J. Hwang, T. Ohsaka, B.-J. Kim, T.-Y. Kim, Y.-G. Yoon, Z. Chen, M.H. Seo, B. Han, *Nanoscale*, (2017), 9, 7373-7379.
- 29) T.C. Chen, M.Q. Zhao, Q. Zhang, G.L. Tian, J.Q. Huang, F. Wei, *Adv. Funct. Mater.*, (2013), 23, 5066-5073.
- 30) X.H. Li, M. Antonietti, *Angew. Chem., Int. Ed.*, (2013), 52, 4572-4576.
- 31) X. Duan, S. Indrawirawan, H. Sun, S. Wang, *Catalysis Today*, (2015), 249, 184-191.
- 32) B. Hinnemann, P.G. Moses, J. Bonde, K.P. Jørgensen, J.H. Nielsen, S. Hørch, I. Chorkendorff, J.K. Nørskov, *J. Am. Chem. Soc.*, (2005), 127, 5308-5309.
- 33) J. Kang, J. Hwang, B. Han, *J. Phys. Chem. C*, (2018).
- 34) D.-Y. Wang, M. Gong, H.-L. Chou, C.-J. Pan, H.-A. Chen, Y. Wu, M.-C. Lin, M. Guan, J. Yang, C.-W. Chen, *J. Am. Chem. Soc.*, (2015), 137, 1587-1592.
- 35) D.-H. Ha, B. Han, M. Risch, L. Giordano, K.P. Yao, P. Karayaylali, Y. Shao-Horn, *Nano Energy*, (2016), 29, 37-45.
- 36) E.J. Popczun, J.R. McKone, C.G. Read, A.J. Bicchi, A.M. Wiltrout, N.S. Lewis, R.E. Schaak, *J. Am. Chem. Soc.*, (2013), 135, 9267-9270.
- 37) J. Deng, P. Ren, D. Deng, L. Yu, F. Yang, X. Bao, *Energy Environ. Sci.*, (2014), 7, 1919-1923.
- 38) D. Merki, H. Vrubel, L. Rovelli, S. Fierro, X. Hu, *Chemical Science*, (2012), 3, 2515-2525.
- 39) M. Tavakkoli, T. Kallio, O. Reynaud, A.G. Nasibulin, C. Johans, J. Sainio, H. Jiang, E.I. Kauppinen, K. Laasonen, *Angew. Chem.*, (2015), 127, 4618-4621.
- 40) J. Deng, P. Ren, D. Deng, X. Bao, *Angew. Chem., Int. Ed.*, (2015), 54, 2100-2104.
- 41) X. Zou, X. Huang, A. Goswami, R. Silva, B.R. Sathe, E. Mikmeková, T. Asefa, *Angew. Chem.*, (2014), 126, 4461-4465.
- 42) H. Zhang, Z. Ma, J. Duan, H. Liu, G. Liu, T. Wang, K. Chang, M. Li, L. Shi, X. Meng, *ACS Nano*, (2015), 10, 684-694.
- 43) D. Deng, L. Yu, X. Chen, G. Wang, L. Jin, X. Pan, J. Deng, G. Sun, X. Bao, *Angew. Chem., Int. Ed.*, (2013), 52, 371-375.
- 44) S.H. Noh, M.H. Seo, J. Kang, T. Okajima, B. Han, T. Ohsaka, *NPG Asia Mater.*, (2016), 8, e312.
- 45) Y. Hu, J.O. Jensen, W. Zhang, L.N. Cleemann, W. Xing, N.J. Bjerrum, Q. Li, *Angew. Chem., Int. Ed.*, (2014), 53, 3675-3679.
- 46) Y. Hou, T. Huang, Z. Wen, S. Mao, S. Cui, J. Chen, *Adv. Energy Mater.*, (2014), 4.
- 47) H.T. Chung, J.H. Won, P. Zelenay, *Nat. Commun.*, (2013), 4, 1922.
- 48) J. Snyder, T. Fujita, M. Chen, J. Erlebacher, *Nat. Mater.*, (2010), 9, 904.
- 49) X. Cui, P. Ren, D. Deng, J. Deng, X. Bao, *Energy Environ. Sci.*, (2016), 9, 123-129.
- 50) Y. Lee, J. Suntivich, K.J. May, E.E. Perry, Y. Shao-Horn, *J. Phys. Chem. Lett.*, (2012), 3, 399-404.
- 51) Y. Feng, X.-Y. Yu, U. Paik, *Sci. Rep.*, (2016), 6, 34004.
- 52) B. Wang, *J. Power Sources*, (2005), 152, 1-15.
- 53) S. Kattel, G. Wang, *J. Phys. Chem. Lett.*, (2014), 5, 452-456.
- 54) J. Zhang, Z. Wang, Z. Zhu, *J. Power Sources*, (2014), 255, 65-69.
- 55) Z. Hou, X. Wang, T. Ikeda, K. Terakura, M. Oshima, M.-a. Kakimoto, S. Miyata, *Phys. Rev. B*, (2012), 85, 165439.
- 56) A.L.P. Silva, L.F. de Almeida, A.L.B. Marques, H.R. Costa, A.A. Tanaka, A.B.F. da Silva, J.d.J.G.V. Júnior, *J. Mol. Model.*, (2014), 20, 2131.
- 57) C.E. Szakacs, M. Lefèvre, U.I. Kramm, J.-P. Dodelet, F. Vidal, *Phys. Chem. Chem. Phys.*, (2014), 16, 13654-13661.
- 58) A. Zitolo, V. Goellner, V. Armel, M.-T. Sougrati, T. Mineva, L. Stievano, E. Fonda, F. Jaouen, *Nat. Mater.*, (2015), 14, 937.
- 59) H. Kim, K. Lee, S.I. Woo, Y. Jung, *Phys. Chem. Chem. Phys.*, (2011), 13, 17505-17510.
- 60) H. Wang, T. Maiyalagan, X. Wang, *ACS Catal.*, (2012), 2, 781-794.
- 61) J. Zhang, Z. Zhao, Z. Xia, L. Dai, *Nat. Nanotechnol.*, (2015), 10, 444.

- 62) J. Deng, L. Yu, D. Deng, X. Chen, F. Yang, X. Bao, *J. Mater. Chem. A*, **(2013)**, 1, 14868-14873.
- 63) S.H. Noh, D.H. Kwak, M.H. Seo, T. Ohsaka, B. Han, *Electrochim. Acta*, **(2014)**, 140, 225-231.
- 64) S.H. Noh, M.H. Seo, X. Ye, Y. Makinose, T. Okajima, N. Matsushita, B. Han, T. Ohsaka, *J. Mater. Chem. A*, **(2015)**, 3, 22031-22034.